

Many-body effects in van der Waals-Casimir interaction between graphene layers

Jalal Sarabadani,^{1,2,*} Ali Naji,^{3,4,†} Reza Asgari,^{4,‡} and Rudolf Podgornik^{2,5,§}

¹*Department of Physics, University of Isfahan, Isfahan 81746, Iran*

²*Department of Theoretical Physics, J. Stefan Institute, SI-1000 Ljubljana, Slovenia*

³*Department of Applied Mathematics and Theoretical Physics, Centre for Mathematical Sciences, University of Cambridge, Cambridge CB3 0WA, United Kingdom*

⁴*School of Physics, Institute for Research in Fundamental Sciences (IPM), Tehran 19395-5531, Iran*

⁵*Institute of Biophysics, School of Medicine and Department of Physics, Faculty of Mathematics and Physics, University of Ljubljana, SI-1000 Ljubljana, Slovenia*

(Dated: January 22, 2013)

Van der Waals-Casimir dispersion interactions between two apposed graphene layers, a graphene layer and a substrate, and in a multilamellar graphene system are analyzed within the framework of the Lifshitz theory. This formulation hinges on a known form of the dielectric response function of an undoped or doped graphene sheet, assumed to be of a random phase approximation form. In the geometry of two apposed layers the separation dependence of the van der Waals-Casimir interaction for both types of graphene sheets is determined and compared with some well known limiting cases. In a multilamellar array the many-body effects are quantified and shown to increase the magnitude of the van der Waals-Casimir interactions.

I. INTRODUCTION

Graphene appears to be the only known mono-atomic two-dimensional (2D) crystal and apart from the intrinsic interest it engenders, it is becoming more and more also a focus of possible and desired advanced technological applications¹. It is for these reasons that in the past several years we have witnessed a veritable explosion of theoretical and experimental interest in graphene². The Nobel prize for physics in 2010 only consolidated this trend. Graphene differs fundamentally from other known 2D semiconductors because of its unique electronic band structure, viz. the monoatomic sheet of carbon atoms arranged in a honeycomb lattice leads to an electron band structure that displays quite unusual properties³. The Fermi surface is reduced to just two points in the Brillouin zone and the value of the band gap is reduced to zero. The energy dispersion relation for both the conduction and the valence bands are linear at low energy, namely less than 1 eV, meaning that the charge carriers behave as relativistic particles with zero rest mass. The agent responsible for many of the interesting electronic properties of graphene sheets is the non-Bravais honeycomb-lattice arrangement of carbon atoms, which leads to a gapless semiconductor with valence and conduction π -bands.

States near the Fermi energy of a graphene sheet are described by a massless Dirac equation which has chiral band states in which the honeycomb-sublattice pseudospin is aligned either parallel or opposite to the envelope function momentum. The Dirac-like wave equation leads to both unusual electron-electron interaction effects and to unusual response to external potentials. When the graphene sheet is chemically doped with either acceptor or donor impurities its carrier mobility can be drastically decreased⁴. Because of its 2D periodic structure graphene is closely related to single wall carbon nanotubes, being in fact a carbon nanotube rolled

out into a single 2D sheet⁵. The main difference between the electronic properties of single wall carbon nanotubes and graphene is that the former show circumferential periodicity and curvature that leave their imprint also in the electronic spectrum and consequently also van der Waals (vdW) interactions^{6,7}.

On the other hand, graphite appears to be the poor cousin of graphene though it is the stable form of carbon at ordinary temperatures and pressures. Many efforts have been invested into understanding its structural and electronic details (for an account see Ref.⁸). Various known modifications of graphite differ primarily in the way the mono-atomic two-dimensional graphene layers stack. Their stacking sequence in terms of commonality is ABA for the Bernal structure, AAA for simple hexagonal graphite or ABC for the rhombohedral graphite⁹.

Graphene layers in graphitic systems are basically closed shell systems and thus have no covalent bonding between layers which makes them almost a perfect candidate to study long(er) ranged non-bonding interactions. Indeed, they are stacked at an equilibrium interlayer spacing of about 0.335 nm and are held together primarily by the non-bonding long range vdW interactions¹⁰. Therefore the interaction between graphene layers can be described as a balance between attractive vdW dispersion forces and corrugated repulsive (Pauli) overlap forces¹¹, following in this respect closely the paradigm of nano-scale interactions¹².

Besides a few notable exceptions¹³, until 2009 many electronic and optical properties of graphene could be explained within a single-particle picture in which electron-electron interactions are completely neglected. The discovery of the fractional quantum Hall effect in graphene¹⁴ represents an important hallmark in this context. By now there is a large body of experimental work^{15–17} showing the relevance of electron-electron interactions in a number of key properties of graphene samples of sufficiently high quality.

Because of band chirality, the role of electron-electron interactions in graphene sheets differs in some essential ways^{18–20} from the role which it plays in an ordinary 2D electron gas. One important difference is that the contribution of exchange and correlation to the chemical potential is an increasing rather than a decreasing function of carrier density. This property implies that exchange and correlation increases the effectiveness of screening, in contrast to the usual case in which exchange and correlation weakens screening²¹. This unusual property follows from the difference in sublattice pseudospin chirality between the Dirac model's negative energy valence band states and its conduction band states^{18,19}, and in a uniform graphene system is readily accounted for by many-body perturbation theory.

In this work we focus our efforts on the vdW dispersion component of the graphene stacking interaction. Dispersion forces can be formulated on various levels²² giving mostly consistent results for their strength and separation dependence. In the context of graphene stacking interactions, the problem can be decomposed into the calculation of the dielectric response of the carbon sheets and the subsequent calculation of the vdW interactions either via the quantum-field-theory-based Lifshitz approach, as advocated in this paper, by means of the electron correlation energy²³ or the non-local vdW density functional theory²⁴. One can show straightforwardly that in fact the non-local van der Waals functional approach of the density functional theory and the Lifshitz formalism are in general equivalent²⁵.

Specifically we will calculate the vdW-Casimir interaction free energy, per unit area between two graphene sheets as a function of the separation between them, in a system composed of

- a) two apposed undoped or doped graphene sheets,
- b) an undoped or a doped graphene layer over a semi-infinite substrate, and

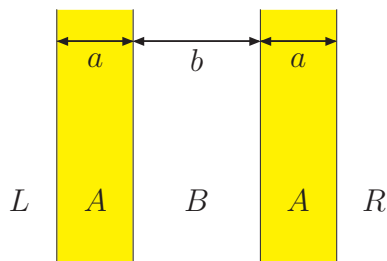


FIG. 1: (Color online) Schematic presentation of two graphene sheets of finite thickness immersed in vacuo at a separation of b . The thickness of both (left and right) layers are equal to a . In view of later generalizations, we have labeled the left semi-infinite vacuum layer with L , the graphene layers with A , the intervening vacuum layer with B and the right vacuum layer with R . The form of the dielectric functions of the graphene layers is given in Eq. (8).

- c) a multilayer (infinite) array of graphene sheets.

In the latter case we will investigate the many-body non-pairwise additive effects in the effective interaction between two sheets within a multilayer array. We should note that non-pairwise additive effects are ubiquitous in the context of vdW interactions²² often leading to non-trivial properties of macromolecular interactions. In this case they will lead to variations in the equilibrium stacking separation as a function of the number of layers in a graphitic configuration. In the calculation of the vdW-Casimir free energy we will employ the dielectric response function of a single graphene layer calculated previously¹⁸.

II. VDW-CASIMIR INTERACTION BETWEEN TWO LAYERS OF GRAPHENE

The geometry of the system composed of two parallel graphene layers with thicknesses a , facing each other in a bilayer arrangement at a separation b , is shown schematically in Fig. 1. In view of later generalizations we label the left semi-infinite vacuum space as L , graphene sheets as A , the intervening layer as B and the right semi-infinite vacuum space by R .

In order to calculate the vdW-Casimir dispersion interaction free energy in the planar geometry we use the approach of Ref.²⁶ where it has been calculated *exactly* for a multilayer planar geometry. The thus derived general form of the interaction free energy per unit area includes retardation effects and is therefore valid for any spacing between the layers.

For the system which is shown schematically in Fig. 1, the vdW-Casimir interaction free energy is obtained in the Lifshitz form as

$$\frac{F_{gg}(b)}{S} = k_B T \sum_{\mathbf{Q}} \sum_{n=0}^{\infty}{}' \ln \left[1 + \frac{\mathcal{D}_1(i\xi_n)}{\mathcal{D}_2(i\xi_n)} e^{-2b\kappa_B(i\xi_n)} \right], \quad (1)$$

where $F_{gg}(b)$ stands for the graphene-graphene interaction free energy as a function of the layer spacing b (normalized in such a way that it tends to zero at infinite interlayer separation). In the above Lifshitz formula the \mathbf{Q} summation is over the transverse wave vector and the n summation (where the prime indicates that the $n = 0$ term has a weight of $1/2$) is over the imaginary Matsubara frequencies

$$\xi_n = \frac{2\pi n k_B T}{\hbar}, \quad (2)$$

where k_B is the Boltzmann constant, T is the absolute temperature, and \hbar is the Planck constant divided by 2π . All the quantities in the bracket depend on \mathbf{Q} as well as ξ_n .

The other quantities entering the Lifshitz formula are defined as

$$\begin{aligned}
\mathcal{D}_1(\imath\xi_n) &= \Delta_{BA}(\imath\xi_n)\Delta_{AB}(\imath\xi_n) + e^{-2a\kappa_A(\imath\xi_n)}\Delta_{BA}(\imath\xi_n)\Delta_{RA}(\imath\xi_n) + \\
&\quad + e^{-2a\kappa_A(\imath\xi_n)}\Delta_{AL}(\imath\xi_n)\Delta_{AB}(\imath\xi_n) + e^{-4a\kappa_A}\Delta_{AL}\Delta_{RA}, \\
\mathcal{D}_2(\imath\xi_n) &= 1 + e^{-2a\kappa_A(\imath\xi_n)}\Delta_{AB}(\imath\xi_n)\Delta_{RA}(\imath\xi_n) + e^{-2a\kappa_A(\imath\xi_n)}\Delta_{AL}(\imath\xi_n)\Delta_{AB}(\imath\xi_n) \\
&\quad + e^{-4a\kappa_A(\imath\xi_n)}\Delta_{AL}(\imath\xi_n)\Delta_{BA}(\imath\xi_n)\Delta_{AB}(\imath\xi_n)\Delta_{RA}(\imath\xi_n),
\end{aligned} \tag{3}$$

with

$$\Delta_{i\ i-1}(\imath\xi_n) = \frac{\epsilon_i(\imath\xi_n)\kappa_{i-1}(\imath\xi_n) - \epsilon_{i-1}(\imath\xi_n)\kappa_i(\imath\xi_n)}{\epsilon_i(\imath\xi_n)\kappa_{i-1}(\imath\xi_n) + \epsilon_{i-1}(\imath\xi_n)\kappa_i(\imath\xi_n)}, \tag{4}$$

where $\Delta_{i\ i-1}$ quantifies the dielectric discontinuity between homogeneous dielectric layers in the system, where a layer labeled by $i-1$ is located to the left hand side of the layer labeled by i (for details see Ref.²⁶). Also $\kappa_i(\imath\xi_n)$ for each electromagnetic field mode within the material i is given by

$$\kappa_i^2(\imath\xi_n) = Q^2 + \frac{\epsilon_i(\imath\xi_n)\mu_i(\imath\xi_n)\xi_n^2}{c^2}, \tag{5}$$

where c is the speed of light in vacuo, Q is the magnitude of the transverse wave vector, and $\epsilon_i(\imath\xi_n)$ and $\mu_i(\imath\xi_n)$ are the dielectric function and the magnetic permeability of the i -th layer at imaginary frequencies, respectively. For the sake of simplicity we assume that for all layers $\mu_i(\imath\xi_n) = 1$ and that the dielectric function for vacuum layers equals to 1 for all frequencies.

Note that $\epsilon_i(\imath\xi)$ is standardly referred to as the vdW-London transform of the dielectric function and is defined via the Kramers-Kronig relations as²⁷

$$\epsilon(\imath\xi) = 1 + \frac{2}{\pi} \int_0^\infty \frac{\omega\epsilon''(\omega)}{\omega^2 + \xi^2} d\omega. \tag{6}$$

It characterizes the magnitude of spontaneous electromagnetic fluctuations at frequency ξ . In general $\epsilon(\imath\xi)$ is a real, monotonically decaying function of the imaginary argument ξ (for details see Parsegian's book in Ref.²²).

In order to proceed one needs the vdW-London transform of the dielectric function of all layers in the system. The detailed Q - and ω -dependent form of the dielectric function for undoped and/or doped graphene layers are introduced in Secs. II A and II B.

A. Two undoped graphene layers

We employ the response function of a graphene layer from Refs.^{18,28} which for doped graphene assumes the

form

$$\begin{aligned}
\chi(Q, \imath\xi_n, \mu \neq 0) &= -\frac{g\mu}{2\pi\hbar^2 v^2} - \frac{gQ^2}{16\hbar\sqrt{\xi_n^2 + v^2 Q^2}} + \\
&\quad + \frac{gQ^2}{8\pi\hbar\sqrt{\xi_n^2 + v^2 Q^2}} \text{Re} \left[\arcsin \left(\frac{2\mu + \imath\xi_n\hbar}{vQ\hbar} \right) \right. \\
&\quad \left. + \frac{2\mu + \imath\xi_n\hbar}{vQ\hbar} \sqrt{1 - \left(\frac{2\mu + \imath\xi_n\hbar}{vQ} \right)^2} \right], \tag{7}
\end{aligned}$$

where $g = 4$, $v \approx 10^6$ m/s is the Fermi velocity in graphene layer and $\mu = \epsilon_F = \hbar v k_F$ is the chemical potential, ϵ_F the Fermi energy, and $\hbar k_F$ is the Fermi momentum, where $k_F = (4\pi\rho/g)^{1/2}$ and ρ is the the average electron density.

To begin with, we assume that two layers are decoupled and ignore the interlayer Coulomb interaction. The vdW-London dispersion transform of the dielectric function on the level of the *random phase approximation* (RPA) is then given by

$$\epsilon(Q, \imath\xi_n) = 1 - V(Q)\chi(Q, \imath\xi_n, \mu \neq 0), \tag{8}$$

where $V(Q)$ is the (transverse) 2D Fourier-Bessel transform of the Coulomb potential, $V(Q) = \frac{2\pi e^2}{4\pi\epsilon_0\epsilon_m Q}$, e is the electric charge of electron, ϵ_0 is the permittivity of the vacuum and ϵ_m is the average of the dielectric constant for the surrounding media which is equal to 1 for vacuum. In what follows we furthermore assume that to the lowest order the dielectric properties of the graphene layers are not affected by the variation of the separation between them. This assumption is also consistent with the Lifshitz theory that presumes complete independence of the dielectric response functions of the interacting layers.

For undoped graphene layer, i.e. $\rho = 0$, the expression for the vdW-London dispersion transform of the dielectric function simplifies substantially and assumes the form

$$\epsilon(Q, \imath\xi_n) = 1 + \frac{\pi\alpha g c Q}{8\epsilon_m v \sqrt{(\frac{\xi_n}{v})^2 + Q^2}}, \tag{9}$$

where α is the electromagnetic fine-structure constant $\alpha = \frac{e^2}{4\pi\epsilon_0\hbar c} \approx \frac{1}{137}$. It should be noted that, in general, a model going beyond the RPA is necessary in order to account for enhanced correlation effects that would be present in an undoped system²⁹. In this paper, however, we restrict ourselves to the RPA approximation and analyze its predictions in detail.

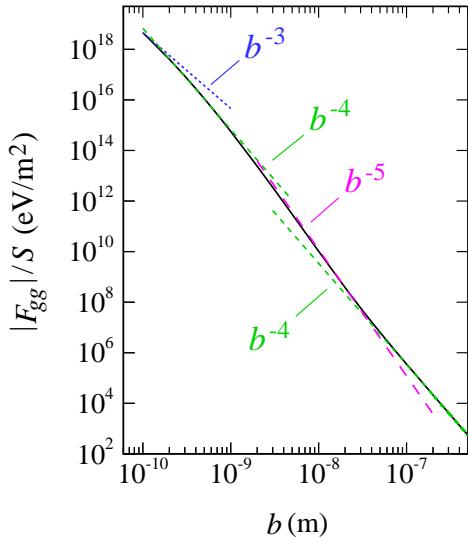


FIG. 2: (Color online) Magnitude of the interaction free energy per unit area of the system composed of two undoped graphene layers immersed in vacuo at an interlayer spacing b , and at temperature 300 K. The functional dependence of the interaction free energy on b is compared with the following scaling forms: b^{-3} , b^{-4} , b^{-5} and b^{-4} as the separation increases.

The functional dependence of the interaction free energy of the system per unit area, Eq. (1), is presented in Fig. 2 as a function of the separation between two graphene layers. We assume that the graphene layers are immersed in vacuo and both of them have the same thickness 1\AA as well as equal susceptibilities. Note that in all cases considered in this paper the interaction free energies as defined in Eq. (1) are negative reflecting attractive vdW-Casimir force between graphene layers in vacuum. For the sake presentation, we shall plot the absolute value (magnitude) of the free energy in all cases.

As one can discern from Fig. 2 the general dependence of the vdW-Casimir interaction free energy on the separation between the graphene layers has the scaling form of a power law, b^{-n} , with a weakly varying separation-dependent scaling exponent, $n(b)$. This scaling exponent can be defined standardly as²²

$$n(b) = -\frac{d \ln F_{gg}(b)}{d \ln b}. \quad (10)$$

For two undoped graphene sheets we observe that at small separations the functional dependence of the free energy on interlayer spacing yields the scaling exponent $n = 3$ for smallest values of the separation. The scaling exponent then steadily increases to $n = 4$, then $n = 5$, and finally at asymptotically large separations it reverts back to $n = 4$. This variation in the scaling exponent for the separation dependence of the interaction free energy can be rationalized by invoking some well known results

on the vdW interaction in multilayer geometries (see e.g. the relevant discussions in Ref.²²).

For example, for two semi-infinite layers the interaction free energy should go from the non-retarded form characterized by $n = 2$ for small spacings, through retarded $n = 3$ form for larger spacings and then back to zero-frequency-only form that also scales with $n = 2$ but with a different prefactor than the non-retarded form. For two infinitely thin sheets, on the other hand, we have the non-retarded $n = 4$ form for small separation, followed by the retarded $n = 5$ form for larger spacings and then reverting back to zero-frequency-only term with $n = 4$ scaling, but again with a different prefactor than the non-retarded limit. Furthermore, the transitions between various scaling forms and the locations of the transition regions are not universal but depend crucially on the characteristics of the dielectric spectra and can thus be quite complicated, sometimes not yielding any easily discernible regimes with a quasi-constant scaling exponent n .

Reading Fig. 2 with this in mind we can come up with the following interpretation of the calculated separation dependence: for small separation the interaction free energy is dominated by the $n = 4$ dependence except in the narrow interval very close to vanishing separation where the dependence asymptotically levels off at $n < 4$ form. This form is consistent with the non-retarded interaction between two very thin layers, see above, for small but not vanishing separations. For vanishing interlayer separations the final leveling-off of the scaling exponent is due to the fact that the system is approaching the limit of two semi-infinite layers where in principle $n \rightarrow 2$, but in reality the finite thickness of the graphene sheets is way too small to observe this scaling in its pure form. All we can claim is that for vanishing interlayer spacings the scaling exponent drops below the $n = 4$ value, valid for two infinitely thin layers.

For larger values of the interlayer separations we then enter the retarded regime with $n = 5$ scaling exponent, again valid strictly for two infinitely thin layers. The retarded regime finally gives way to the regime of asymptotically large spacings where the interaction free energy limits towards its form given by the zero frequency term in the Matsubara summation and characterized by $n = 4$ scaling dependence. Obviously the numerical coefficient in the small separation non-retarded and asymptotically large separation regimes (both with $n = 4$) are necessarily different.

The interaction free energy scaling with the interlayer separation is thus completely consistent with the vdW-Casimir interactions between two thin dielectric layers for all, except for vanishingly small, separations where finite thickness effects of the graphene sheets leave their mark in a smaller value of the scaling exponent that should ideally approach the value valid for a regime of interaction between two semi-infinite layers.

The numerical value of the interaction free energy per unit area at 1 nm is about $5.64 \times 10^{14} \text{ eV/m}^2$. That

means that for two graphene layers with surface area of 10^{-12} m^2 the magnitude of the free energy is about 564 eV at 1 nm separation; at 10 nm it is about 0.01 eV and at 100 nm about $3.6 \times 10^{-7} \text{ eV}$ for the same surface area.

B. Two doped graphene layers

For a doped graphene layer the vdW-London dispersion transform of the dielectric function can be read off from Eqs. (8) and (7) as

$$\begin{aligned} \epsilon(Q, \imath\xi_n, \mu \neq 0) = & 1 + \frac{2\pi\alpha c}{\epsilon_m Q v} \sqrt{\frac{\rho g}{\pi}} \\ & + \frac{\pi\alpha g c Q}{8\epsilon_m v \sqrt{(\frac{\xi_n}{v})^2 + Q^2}} \\ & - \frac{\alpha g c Q}{4\epsilon_m v \sqrt{(\frac{\xi_n}{v})^2 + Q^2}} \left\{ \arcsin \left[\frac{1}{2}A_1 - \frac{1}{2}B_1 \right] \right. \\ & + 2\sqrt{\frac{4\pi\rho/g}{Q}} (A_2^2 + B_2^2)^{1/4} \cos \left[\frac{1}{2} \arg(A_2 + \imath B_2) \right] \\ & \left. - \frac{\xi_n}{vQ} (A_2^2 + B_2^2)^{1/4} \sin \left[\frac{1}{2} \arg(A_2 + \imath B_2) \right] \right\}, \quad (11) \end{aligned}$$

with the following coefficients

$$\begin{aligned} A_1 &= \sqrt{\left(\frac{2\sqrt{4\pi\rho/g}}{Q} + 1 \right)^2 + \left(\frac{\xi_n}{vQ} \right)^2}, \\ B_1 &= \sqrt{\left(\frac{2\sqrt{4\pi\rho/g}}{Q} - 1 \right)^2 + \left(\frac{\xi_n}{vQ} \right)^2}, \\ A_2 &= 1 + \left(\frac{\xi_n}{vQ} \right)^2 - 16 \frac{\pi\rho}{gQ^2}, \\ B_2 &= -4 \frac{\xi_n \sqrt{4\pi\rho/g}}{vQ^2}. \quad (12) \end{aligned}$$

With this dielectric response function we again evaluate the vdW-Casimir interaction free energy of the system per unit area, Eq. (1), as a function of the separation between two graphene layers b as shown in Fig. 3. The interaction free energy has again a scaling form with a scaling exponent varying with the separation between the layers. It is clear that in this case it is much more difficult to partition the variation of the scaling exponent into clear-cut piecewise constant regions.

As it can be seen from Fig. 3 at small separations the form of the functional dependence of the interaction free energy has $n < 3$. Then for increasing spacings there follows a relatively broad regime with $n = 3 - 4$, followed eventually by the scaling form with $n = 2$ for $b > 5 \times 10^{-6} \text{ m}$. One needs to add here that only the scaling regime of $n = 2$ for asymptotically large separations and an intermediate regime with $n = 3 - 4$ are clearly discernible.

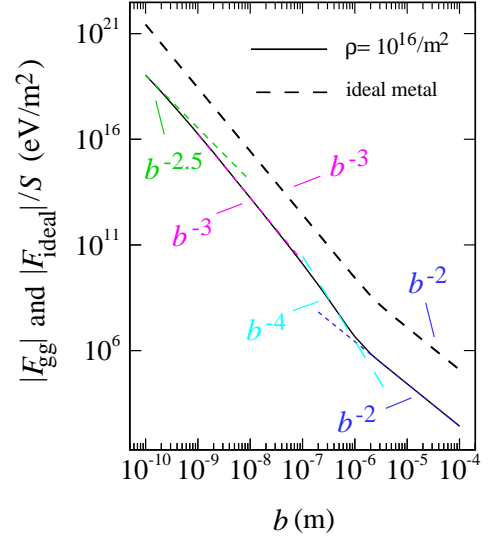


FIG. 3: (Color online) Magnitude of the interaction free energy per unit area of the system composed of two doped graphene layers (solid curve) compared with that of two ideal metallic sheets (dashed curve) immersed in vacuo as a function of the interlayer spacing b , at temperature 300 K. The functional dependence of the free energy on the interlayer spacing is compared with scaling forms $b^{-2.5}$, b^{-3} , b^{-4} and b^{-2} in various regimes of separation.

We can gain some understanding of these regimes by comparing with the various exact limits in the layer geometry as before. Such comparison is however not as straightforward as before. The asymptotic $n = 2$ regime is easiest to rationalize: it has the same scaling form as the *finite temperature* vdW-Casimir interaction between two metallic sheets at asymptotically large separations. The presence of free charges would in fact be a reasonable characterization of doped graphene layers. For smaller separations we then enter the regime dominated by the retardation effects with $n \simeq 3 - 4$ form, and finally for vanishing separations we approach the regime of $n = \frac{5}{2}$. Recent calculations of vdW interactions between thin metallic layers indeed lead to exactly this exponent for small layer separations³¹. The doped graphene sheet results would thus indicate that the dependence of the vdW-Casimir interactions free energy on the separation could be rationalized in terms of interactions between two thin metallic sheets.

For comparison we have also plotted the interaction free energy between two *ideal* metallic sheets which exhibits a much stronger attractive interaction free energy,

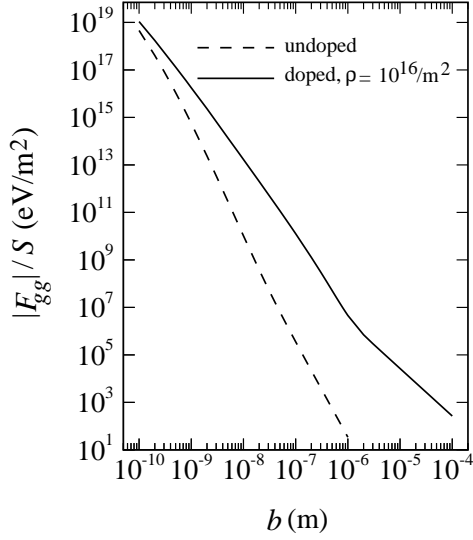


FIG. 4: Magnitude of the free energy per unit area of the system composed of two undoped (dashed line) and doped (solid line) graphene layers (with the electron density $\rho = 10^{16}/\text{m}^2$) immersed in vacuo as a function of the interlayer spacing b , at temperature 300 K. As seen for all separations the magnitude of the interaction free energy for doped graphene layers is greater than that of the undoped one.

i.e.²²

$$\begin{aligned} \frac{F_{\text{ideal}}}{S} &= k_B T \sum_{n=-\infty}^{\infty} \int \frac{d^2 p}{(2\pi)^2} \ln [1 - e^{-2b\sqrt{p^2 + (\xi_n/c)^2}}] \\ &= -\frac{k_B T \zeta(3)}{8\pi b^2} + 2k_B T \times \\ &\quad \times \sum_{n=1}^{\infty} \int \frac{d^2 p}{(2\pi)^2} \ln [1 - e^{-2b\sqrt{p^2 + (\xi_n/c)^2}}]. \end{aligned} \quad (13)$$

The numerical value of the energy per unit area at 1 nm is about $1.77 \times 10^{16} \text{ eV/m}^2$ which is equal to $1.77 \times 10^4 \text{ eV}$ for surface area of 10^{-12} m^2 ; at 10 nm it is about 16.9 eV and at 100 nm it is about 0.01 eV for the same surface area.

C. Doped vs. undoped graphene

It is instructive to compare the interaction between two graphene layers in the undoped and doped cases. For this purpose we have plotted the interaction free energy of the system for both cases in Fig. 4. The electron density in doped graphene is assumed to be $\rho = 10^{16}/\text{m}^2$ (solid curve). The dashed curve is the interaction free energy of the system composed of two undoped graphene layers. As it can be seen, for all separations the magnitude of the interaction free energy for doped graphene layers is more than that of the undoped one (note again that the

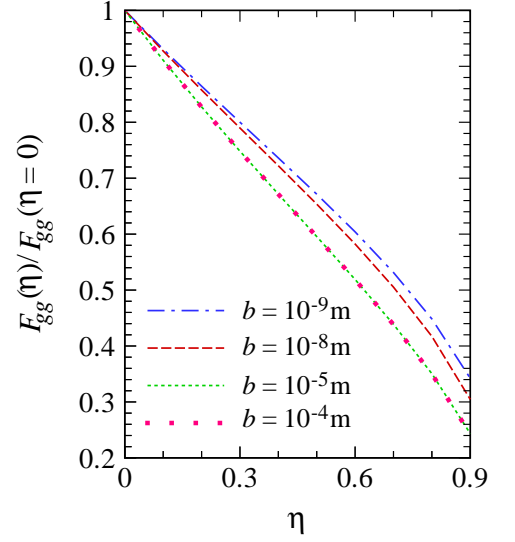


FIG. 5: (Color online) The rescaled interaction free energy, $F_{gg}(\eta)/F_{gg}(\eta = 0)$, for the system composed of two doped graphene layers with different electron densities immersed in vacuum as a function of $\eta = \frac{\rho_1 - \rho_2}{\rho_1 + \rho_2}$ for different interlayer separations $b = 1 \text{ nm}, 10 \text{ nm}, 10 \mu\text{m}$, and $100 \mu\text{m}$ (from top to bottom) at temperature 300 K. Note that $F_{gg}(\eta = 0)$ has been calculated for $\rho_1 = \rho_2 = 10^{16}/\text{m}^2$.

interaction free energies as defined in Eq. (1) are negative in the present case due to attractive vdW-Casimir force between graphene layers in vacuum). At separation 1 nm the vdW-Casimir interactions for doped graphene is about 30 times the magnitude of the interaction for undoped graphene, while at the separation of 10 nm this ratio is about 1600. This means that the attractive interaction between graphene layers is enhanced when the contribution of the electron density in the dielectric function of the graphene layers is taken into account. This same trend was observed also in the work of Sernelius²³ and is clearly a consequence of the fact that the largest value of vdW-Casimir interactions is obtained for ideally polarizable, i.e. metallic layers. The closer the system is to this idealized case, the larger the corresponding vdW-Casimir interaction will be.

Let us investigate also the effect of asymmetry of doped graphene sheets on vdW-Casimir interactions between them. Introducing the dimensionless parameter $\eta = \frac{\rho_1 - \rho_2}{\rho_1 + \rho_2}$, where ρ_i is the electron density of the i -th graphene layer ($i = 1, 2$), we find that the interaction free energy depends on the asymmetry in the system. When $\eta = 0$, the electron densities are the same for both graphene layers and we have a symmetric case, whereas $\eta = 1$ means that one of the graphene layers is undoped while the other one is doped, leading to an asymmetric case. In Fig. 5 we have plotted the rescaled free energy $F_{gg}(\eta)/F_{gg}(\eta = 0)$ of the system composed of two graphene layers as a function of η for different val-

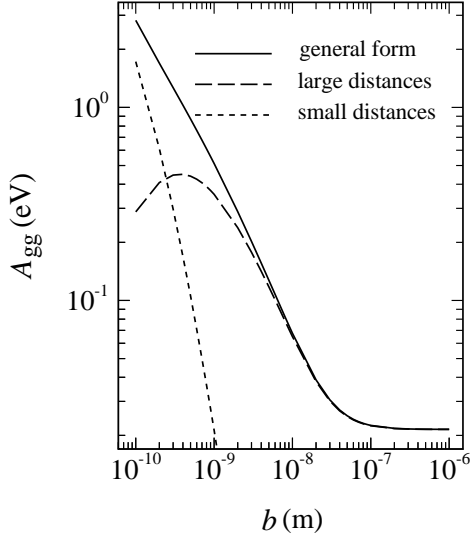


FIG. 6: Hamaker coefficient for a system of two undoped graphene layers as a function of the distance between them, b . The top solid line shows the general form of the Hamaker coefficient as defined via Eq. (14), the dashed line shows the limiting large-distance form, Eq. (15), and the dotted line shows the limiting small-distance form, Eq. (16).

ues of the interlayer separation. The magnitude of the electron density for one of the layers has been fixed at $\rho_1 = 10^{16}/\text{m}^2$ while that of the other layer, ρ_2 , varies. As seen from this figure, the curves show a monotonic dependence on η with a stronger interaction at smaller values of η . Note that at large separations the curves tend to coincide and will become indistinguishable. The asymmetry effects are therefore largest at small separations between the interacting graphene layers.

D. Hamaker coefficient for two graphene layers

The general form of the Hamaker coefficient, A_{gg} , for a system composed of two dielectric layers of finite thickness (Fig. 1) when retardation effects are neglected is defined via²²

$$\frac{F_{gg}(b)}{S} = -\frac{A_{gg}}{12\pi b^2} \left[1 - \frac{2b^2}{(b+a)^2} + \frac{b^2}{(b+2a)^2} \right]. \quad (14)$$

At large separations $b \gg a$, the Hamaker coefficient, A_{gg}^{large} , can be obtained from

$$\frac{F_{gg}(b)}{S} = -\frac{A_{gg}^{\text{large}} a^2}{2\pi b^4}, \quad (15)$$

while at small separations $b \ll a$, it can be read off from

$$\frac{F_{gg}(b)}{S} = -\frac{A_{gg}^{\text{small}}}{12\pi b^2}. \quad (16)$$

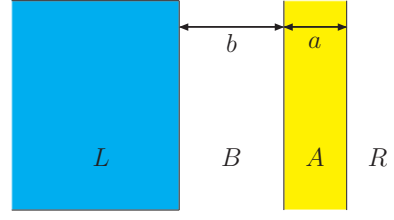


FIG. 7: (Color online) Schematic presentation of a graphene layer of thickness a (labeled by A) apposed to a substrate (labeled by L) at a separation b . We have labeled the intervening layer (assumed to be vacuum) with B , and the right one with R . The dielectric function of the graphene layer is defined via Eq. (8) and for substrate via Eq. (18).

In Fig. 6, we show the Hamaker coefficient as a function of the layer separation for a system of two undoped graphene layers. We show the general form of the Hamaker coefficient from Eq. (14) (solid line) as well as the limiting forms at small (dotted line, Eq. (16)) and large (dashed line, Eq. (15)) separations. The large-distance limiting form obviously coincides with the general form at separations beyond 50 nm. The small-distance limiting form tends to the general form at small separations but given that the thickness of the layers is only about 1\AA , it is expected to merge with the general form in sub-Ångström separations. For doped graphene, a similar analysis to Eq. (14) is not possible because the corresponding general expression for the interaction free energy is missing.

III. VDW-CASIMIR INTERACTION BETWEEN A GRAPHENE LAYER AND A SEMI-INFINITE SUBSTRATE

In this section we study the interaction between a graphene layer and a semi-infinite dielectric substrate as depicted schematically in Fig. 7. For this system the free energy per unit area is

$$\begin{aligned} \frac{F_{sg}(b)}{S} = & k_B T \times \\ & \times \sum_{\mathbf{Q}} \sum_{n=0}^{\infty} \ln \left[1 + \frac{\Delta_{AB} + \Delta_{RA} e^{-2a\kappa_A}}{1 + \Delta_{AB} \Delta_{RA} e^{-2a\kappa_A}} \Delta_{BL} e^{-2b\kappa_B} \right], \end{aligned} \quad (17)$$

where F_{sg} now stands for the interaction free energy between the substrate and the graphene layer. We have excluded the explicit dependence of the quantities in the bracket on the imaginary Matsubara frequencies, but they are the same as in Eq. (4).

In order to gain insight into the magnitude of the vdW-Casimir interaction free energy and for the sake of simplicity, we assume that the semi-infinite substrate is made of SiO_2 which has the vdW-London dispersion transform

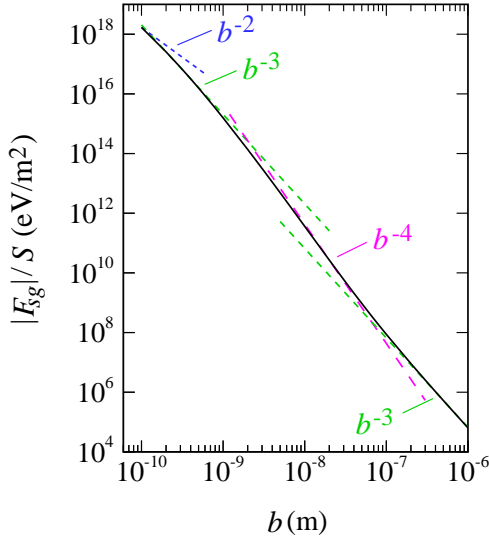


FIG. 8: (Color online) Magnitude of the interaction free energy of the system composed of a SiO₂ substrate and an undoped graphene layer, Eq. (17), plotted at temperature 300 K as a function of the separation b . The functional dependence of the free energy on b is compared with scaling forms b^{-2} , b^{-3} , b^{-4} and b^{-3} in various regimes of separation.

of the dielectric function of the form^{22,32}

$$\epsilon_L(i\xi_n) = 1 + \frac{C_{UV}\omega_{UV}^2}{\xi_n^2 + \omega_{UV}^2} + \frac{C_{IR}\omega_{IR}^2}{\xi_n^2 + \omega_{IR}^2}, \quad (18)$$

where the values of the parameters, $C_{UV} = 1.098$, $C_{IR} = 1.703$, $\omega_{UV} = 2.033 \times 10^{16}$ rad/s, and $\omega_{IR} = 1.88 \times 10^{14}$ rad/s have been determined from a fit to optical data³³. The static dielectric permittivity of SiO₂ is then obtained as $\epsilon(0) = 3.81$. A characteristic feature of the vdW-London transform of SiO₂ is thus that it contains two relaxation mechanisms. The first one is due to electronic polarization and the second one is due to ionic polarization. All calculations of the vdW-Casimir interaction free energy are done at room temperature (300 K).

A. Undoped graphene apposed to a substrate

Using the vdW-London transforms of the dielectric functions given in the preceding sections, one can now calculate the free energy, Eq. (17), for an undoped graphene layer next to a semi-infinite SiO₂ substrate. The results are shown in Fig. 8.

At small separations, the free energy varies with a scaling exponent $n = 2$, while at larger separations one can distinguish the scaling regimes $n = 3$, and $n = 4$, finally approaching the asymptotic limit at large separations with $n = 3$. This sequence of interaction free energy scalings can be rationalized as follows: at asymptotically large separations we are at the zero-frequency Matsubara

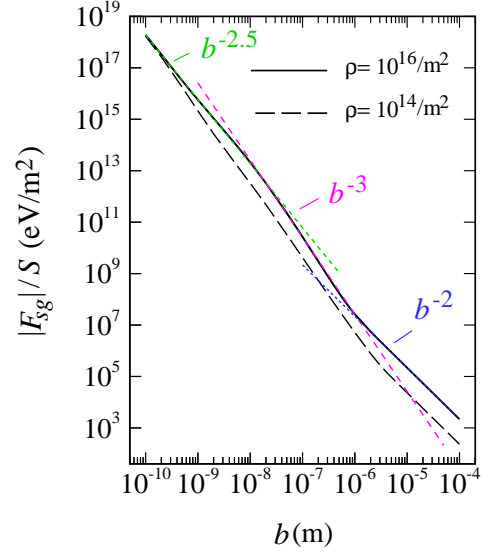


FIG. 9: (Color online) Magnitude of the interaction free energy of the system composed of a SiO₂ substrate and a doped graphene layer, Eq. (17) is plotted at temperature 300 K as a function of the separation b . Here the functional dependence of the interaction free energy for the graphene doping electron density $\rho = 10^{16}/\text{m}^2$ (solid line) is compared with scaling forms $b^{-2.5}$, b^{-3} and b^{-2} in various regimes of separation. We also include the same plot for the doping electron density $\rho = 10^{14}/\text{m}^2$ (dashed line).

term for a semi-infinite layer and a thin sheet. This case is right in between the asymptotically large separation limit for two semi-infinite layers ($n = 2$) and two infinitely thin layers ($n = 4$). For smaller spacings we then progressively detect contributions from higher Matsubara terms which lead to scaling exponent $n = 4$ that corresponds to a retarded form of the interaction free energy and then for yet smaller spacings the scaling exponent reverts to $n = 3$ non-retarded form of the vdW interaction between a semi-infinite substrate and an infinitely thin sheet. For vanishing spacings the finite thickness of the sheet starts playing a role and eventually, we approach the $n = 2$ scaling for two semi-infinite layers.

The magnitude of the interaction free energy per unit area at 1 nm is about 1.57×10^{15} eV/m². It means that for a system with surface area of 10^{-12} m² this value is about 1.57×10^3 eV. At 10 nm it is about 0.36 eV and at 100 nm it is about 8.71×10^{-5} eV for the same surface area.

B. Doped graphene apposed to a substrate

The vdW-Casimir interaction free energy Eq. (17) for a system composed of a doped graphene layer next to a semi-infinite SiO₂ substrate is shown Fig. 9 for two values of the electron density $\rho = 10^{14}/\text{m}^2$ (dashed line)

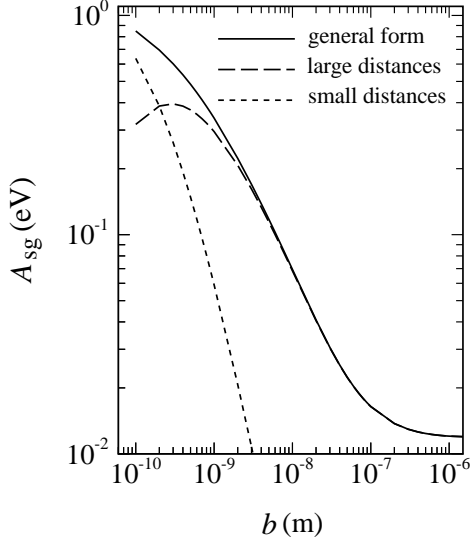


FIG. 10: Hamaker coefficient for a system of an undoped graphene layer apposed to a SiO_2 substrate as a function of the distance between them, b . The top solid line shows the general form of the Hamaker coefficient as defined via Eq. (19), the dashed line show the limiting large-distance form, Eq. (20), and the dotted line shows the limiting small-distance form, Eq. (21).

and $\rho = 10^{16}/\text{m}^2$ (solid line).

At small separations the free energy shows the $n = \frac{5}{2}$ scaling, while for larger spacings it shows a scaling exponent $n = 3$, approaching the $n \rightarrow 2$ limit for asymptotically large separations. In this respect the case of a thin doped graphene sheet apposed to a semi-infinite substrate is very similar to the case of two thin doped layers, except that the retarded regime covers a smaller interval of spacings. This means that the metallic nature of one of the interacting surfaces is enough to switch the behavior of the interaction free energy completely towards the case of two metallic interacting surfaces. This case has in fact not yet been thoroughly discussed in the literature. The changes in the slope appear to occur at the same values of the interlayer spacing when the electron density decreases (compare dashed and solid curves).

The magnitude of the free energy for the electron density $\rho = 10^{14}/\text{m}^2$ (dashed line) and surface area of 10^{-12} m^2 at 1 nm is about $2.12 \times 10^3 \text{ eV}$, while at 10 nm it is about 3.28 eV, and at 100 nm is about $4.20 \times 10^{-3} \text{ eV}$.

These values increase for larger electron densities, e.g., for $\rho = 10^{16}/\text{m}^2$ (solid line) and the same surface area, the free energy magnitude is $5.77 \times 10^3 \text{ eV}$ at 1 nm, while it is about 21.1 eV at 10 nm and about $2.67 \times 10^{-2} \text{ eV}$ at 100 nm.

C. Hamaker coefficient for the graphene-substrate system

The general form of the Hamaker coefficient, A_{sg} , for a system composed of a dielectric layer of finite thickness apposed to a semi-infinite dielectric substrate (Fig. 7) when retardation effects are neglected is defined via²²

$$\frac{F_{sg}(b)}{S} = -\frac{A_{sg}}{12\pi b^2} \left[1 - \frac{b^2}{(b+a)^2} \right]. \quad (19)$$

At large separations $b \gg a$, the Hamaker coefficient, A_{sg}^{large} , can be obtained from

$$\frac{F_{sg}(b)}{S} = -\frac{A_{sg}^{\text{large}} a}{6\pi b^3}, \quad (20)$$

while at small separations $b \ll a$, it can be read off from

$$\frac{F_{sg}(b)}{S} = -\frac{A_{sg}^{\text{small}}}{12\pi b^2}. \quad (21)$$

In Fig. 10, we again show the Hamaker coefficient as a function of the layer separation for a system comprising a SiO_2 substrate and an undoped graphene layer. We show the general form of the Hamaker coefficient from Eq. (19) (solid line) as well as the limiting forms at large (dashed line, Eq. (20)) and small (dotted line, Eq. (21)) separations. The large-distance limiting form obviously coincides with the general form at separations beyond 10 nm but again since the thickness of the graphene layer is only about 1 Å, the small-distance limiting form is expected to merge with the general form in sub-Ångström separations.

IV. VDW-CASIMIR INTERACTION IN A SYSTEM COMPOSED OF $N + 1$ LAYERS OF GRAPHENE

In this section we shall use the Lifshitz formalism in order to study the many-body vdW interactions in a system composed of $N + 1$ layers of graphene. The layers are separated from each other by N layers of vacuum and are bounded at the two ends by two semi-infinite dielectric slabs as depicted in Fig. 11. The thickness of each graphene layer is a while the separation between two successive layers is b . We have labeled the left semi-infinite dielectric medium with L , the right one with R (which both will be assumed to be vacuum), the graphene layers with A and the vacuum layers with B . Following Ref.³⁰, one can calculate the vdW-Casimir part of the interaction free energy, $F_N(a, b)$, in an explicit form for any finite N . Interestingly, it turns out that for very large values of N the vdW-Casimir free energy can be written as a linear function of N so that the interaction free energy $F_N(a, b)$ becomes³⁰

$$F_N(a, b) = N f_{gg}(a, b) \quad N \gg 1, \quad (22)$$

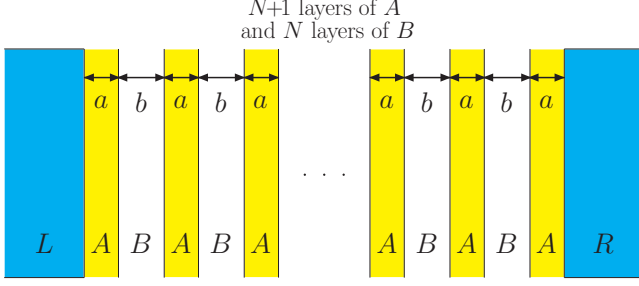


FIG. 11: (Color online) Schematic picture of the system composed of $N + 1$ layers of graphene (A) with equal thicknesses a separated from each other by N layers of vacuum (B) with equal thicknesses of b . The two semi-infinite substrates in the left and right end of the system are labeled by L and R and will be assumed to be vacuum.

where $f_{gg}(a, b)$ can be interpreted as an *effective* pair interaction between two neighboring layers in the stack and is given by

$$f_{gg}(a, b) = k_B T \times \sum_Q \sum_{n=0}^{\infty} \ln \frac{1}{2} \left[\frac{1 - \Delta^2 (e^{-2\kappa_A a} + e^{-2\kappa_B b}) + e^{-2(\kappa_A a + \kappa_B b)}}{(1 - \Delta^2 e^{-2\kappa_A a})} + \sqrt{\frac{\mathcal{G}(a, b, \Delta)}{(1 - \Delta^2 e^{-2\kappa_A a})^2}} \right], \quad (23)$$

with $\mathcal{G}(a, b, \Delta)$ defined as

$$\begin{aligned} \mathcal{G}(a, b, \Delta) = & (1 - e^{-2(\kappa_A a + \kappa_B b)})^2 \\ & - 2\Delta^2 \left[(e^{-2\kappa_A a} + e^{-2\kappa_B b})(1 + e^{-2(\kappa_A a + \kappa_B b)}) \right. \\ & \left. - 4e^{-2(\kappa_A a + \kappa_B b)} \right] + \Delta^4 (e^{-2\kappa_A a} - e^{-2\kappa_B b})^2. \end{aligned} \quad (24)$$

Here Δ is

$$\Delta = \frac{\kappa_A \epsilon_B - \kappa_B \epsilon_A}{\kappa_A \epsilon_B + \kappa_B \epsilon_A}, \quad (25)$$

where κ_A and κ_B are

$$\kappa_{A,B}^2 = Q^2 + \xi_n^2 \epsilon_{A,B} (i\xi_n)/c^2. \quad (26)$$

For simplicity we have dropped the explicit dependence on the Matsubara frequency in all the above expressions. We stress that $f_{gg}(a, b)$ is an effective pair interaction between two neighboring graphene layers in a multilayer geometry and is in general *not* equal to $F_{gg}(a, b)$ in Eq. (1), which is valid for two interacting layers in the absence of any other neighboring layers. The difference between these two interaction free energies thus encodes the non-pairwise additive effects in the interaction between two layers due to the presence of other vicinal layers.

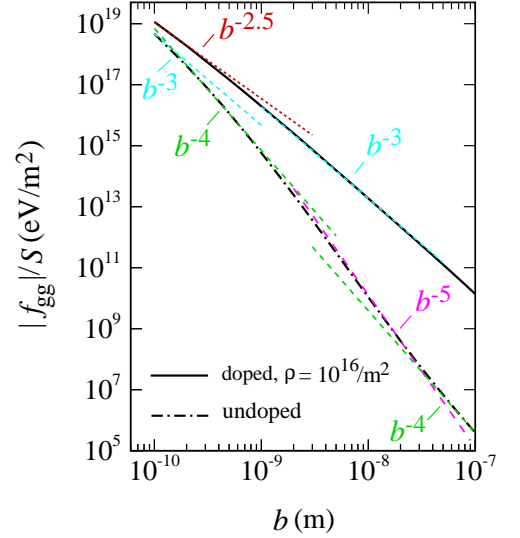


FIG. 12: (Color online) Magnitude of the interaction free energy per unit area and number of layers, $|f_{gg}|/S$, plotted as a function of the separation, b , between two successive undoped (bottom black dot-dashed line) and doped (top black solid line) graphene layers for a system composed of infinitely many layers of undoped/doped layers as schematically depicted in Fig. 11. The temperature of the system is 300 K, the thickness of the graphene layers is fixed at 1 Å and we have chosen the dielectric function for the undoped case from Eq. (9) and for doped case (with the doping electron density chosen as $\rho = 10^{16}/\text{m}^2$) from Eq. (11). The functional form of the free energy for the undoped case is compared with scaling forms b^{-3} , b^{-4} , b^{-5} and b^{-4} in various regimes of separation. For the doped case, the free energy is compared with the scaling forms $b^{-2.5}$ and b^{-3} .

A. $N + 1$ undoped graphene layers

Let us first consider the case of $N+1$ undoped graphene layers. In this case the vdW-Casimir interaction free energy per unit area and per number of layers, $|f_{gg}(b)|/S$ (black dot-dashed line), has been plotted in Fig. 12 as a function of the separation between the layers, b . The temperature of the system is chosen as 300 K, the thickness of the graphene layers is 1 Å and we have used the dielectric function given by Eq. (9) for each undoped graphene sheet.

The value of $|f_{gg}|/S$ at 1 nm is about $5.9 \times 10^{14} \text{ eV/m}^2$ which is $5.9 \times 10^2 \text{ eV}$ when the surface area is equal to 10^{-12} m^2 . At 10 nm the value of $|f_{gg}|$ for the same surface area is about 0.01 eV and at 100 nm is about $3.9 \times 10^{-7} \text{ eV}$.

The scaling of $|f_{gg}(b)|/S$ for different values of the interlayer spacing b is shown in Fig. 12. It shows the scaling exponent $n = 3$ at vanishing separations while at finite yet small separations it is characterised by $n = 4$, continuously merging into a $n = 5$ form and finally attaining the $n = 4$ form. The rationalization of this sequence of

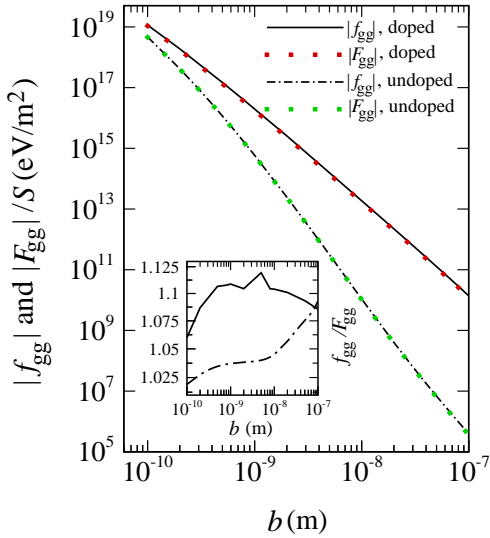


FIG. 13: (Color online) Magnitude of the interaction free energy per unit area and number of layers, $|f_{gg}|/S$, for the system composed of $N + 1$ layers of undoped (bottom black dot-dashed line) and doped (top black solid line) graphene is compared with the magnitude of the interaction free energy per unit area, $|F_{gg}|/S$, for the system composed of only two undoped (green dots) and doped (red dots) graphene layers as a function of the separation between the layers, b . The inset shows the ratio of these two quantities for both undoped (black dot-dashed line) and doped (black solid line) cases.

scaling exponents is exactly the same as in the case of two isolated layers and will thus not be repeated here.

One can directly compare the reduced free energy, $f_{gg}(b)$, with that of a system composed of only two undoped graphene layers of the same thickness a , $F_{gg}(b)$ (i.e., comparing the results in Fig. 2 with the corresponding results in Fig. 12). This is shown in Fig. 13 (black dot-dashed line and green dots), where apparently the results nearly coincide. However, by inspecting the ratio between these two interaction free energies it turns out that in the multilayer system the interaction free energy per layer is slightly more attractive than in the case of a two-layer system. This difference thus stems directly from the many-body effects which in this case augment the binding interaction in a graphitic stack.

B. $N + 1$ doped graphene layers

In Fig. 12 the magnitude of the vdW-Casimir interaction free energy for doped graphene layers per unit area and per number of layers, $|f_{gg}(b)|/S$, is plotted (black solid line) as a function of the separation between layers, b . The vdW-London dispersion transform of the dielectric function for each graphene sheet is chosen as in Eq. (11). We have fixed the density of electrons for

all the graphene layers as $\rho = 10^{16}/\text{m}^2$. The value of $|f_{gg}|/S$ at 1 nm is about 1.96×10^{16} eV/m², which is about 1.96×10^4 eV when the surface area is equal to 10^{-12} m². At 10 nm the value of $|f_{gg}|$ is about 18.7 eV and at 100 nm it is about 1.38×10^{-2} eV. The scaling exponents of the interaction free energy dependence for different regions of interlayer spacings are illustrated in Fig. 12. The scaling exponent is $n = 2.5$ for small separations while at larger separations it tends towards the value $n = 3$. It is thus exactly the same as in the case of two isolated doped graphene sheets, see Fig. 3, except that in the multilayer geometry we have not shown the same range of separations as for two isolated layers.

The comparison of vdW-Casimir interaction free energies in the case of two isolated doped graphene sheets with the effective interaction between two graphene sheets in a multilayer system (i.e., comparing $|F_{gg}|$ in Fig. 3 with $|f_{gg}|$ in Fig. 12) is made in Fig. 13. As shown by the inset the interaction free energy is again slightly more attractive within a multilayer. Comparing the results in the inset of Fig. 13 shows that in average the many-body effects are stronger in the doped multilayer case than in the undoped case.

Note also that a direct comparison between the undoped and doped systems (Fig. 12) shows that for all separations the free energy magnitude for a doped multilayer (solid line) is more than that of the undoped one (dot-dashed line) and thus the interaction is more attractive in the former case. At separation 1 nm the magnitude of the doped free energy is about 34 times larger, while at the separation 10 nm it is about 1730 larger than that of the undoped one.

V. CONCLUSION

In this work we have studied the vdW-Casimir interaction between graphene sheets and between a graphene sheet and a substrate. We calculated the interaction free energy via the Lifshitz theory of vdW interactions that takes as an input the dielectric functions, or better their vdW-London transform, of isolated layers. Within this approach it would be inconsistent to take into account any separation dependent coupling between the dielectric response of the layers. This need possibly not be the case for some other approximate approaches to vdW interactions as in, e.g., the vdW augmented density functional theory (see the paper by Langreth et al. in Ref.²²).

By inserting the *random phase approximation* dielectric function of a graphene layer into the Lifshitz theory we are thus in a position to evaluate not only the pair interaction between two isolated graphene sheets, but also between a graphene sheet and a semi-infinite substrate of a different dielectric nature (SiO₂ in our case) as well as the effective interactions between two graphene sheets in an infinite stack of graphene layers. All these cases that have been analyzed and discussed above are relevant for many realistic geometries in nano-scale systems¹² and

thus deserve to be studied in detail.

In the three cases studied we found the following salient features of the vdW-Casimir interaction dependence on the separation between the interacting bodies:

- 1- In a system composed of two graphene layers we demonstrated that the vdW-Casimir interactions in the case of undoped graphene show scaling exponents identical to those displayed in the case of interacting thin dielectric layers. In the doped case the scaling exponents are consistent with vdW-Casimir interactions between two thin metallic layers.
- 2- In a system composed of a semi-infinite dielectric substrate and an undoped graphene layer the vdW-Casimir interactions display scaling exponents expected for this asymmetric geometry. For a doped graphene layer the exponents revert to the previous case of two doped graphene layers.
- 3- In a multilayer system composed of many graphene sheets the vdW-Casimir interaction scaling exponents are the same as in the case of two isolated layers but the interactions are stronger due to many body effects as a consequence of the presence of other layers in a stack.

In order to describe the correlation effects especially

at low doping or the interlayer coupling on a more systematic level, one needs to go beyond the standard random phase approximation by incorporating more sophisticated theoretical models for the dielectric response function which would be worth exploring further in the future.

The main motivation for a detailed study of vdW-Casimir interaction between graphene sheets in graphite-like geometries is the fact that graphitic systems belong to closed shell systems and thus display no covalent bonding, so that any bonding interaction is by necessity of a vdW-Casimir type. Its detailed characterization is thus particularly relevant for this quintessential nano-scale system¹².

VI. ACKNOWLEDGMENT

We would like to thank B. Sernelius for providing us with a preprint of his work. R.P. acknowledges support from ARRS through the program P1-0055 and the research project J1-0908. A.N. acknowledges support from the Royal Society, the Royal Academy of Engineering, and the British Academy. J.S. acknowledges generous support by J. Stefan Institute (Ljubljana) provided for a visit to the Institute and the Department of Physics of IASBS (Zanjan) for their hospitality.

* Electronic address: j.sarabadani@phys.ui.ac.ir

† Electronic address: a.naji@damtp.cam.ac.uk; (corresponding author)

‡ Electronic address: asgari@ipm.ir

§ Electronic address: rudolf.podgornik@fmf.uni-lj.si

¹ K. S. Novoselov, E. McCann, S. V. Morozov, V. I. Fal'ko, M. I. Katsnelson, U. Zeitler, D. Jiang, F. Schedin, A. K. Geim, *Nature Phys.* **2**, 177 (2006).

² A. K. Geim and K. S. Novoselov, *Nature Materials* **6**, 183 (2007).

³ A. H. Castro Neto, F. Guinea, N. M. R. Peres, K. S. Novoselov and A. K. Geim, *Rev. Mod. Phys.* **81**, 109 (2009).

⁴ J.-H. Chen, C. Jang, S. Adam, M. S. Fuhrer, E. D. Williams and M. Ishigami, *Nature Physics* **4**, 377 (2008).

⁵ R. Saito, G. Dresselhaus, and M. S. Dresselhaus, *Physical Properties of Carbon Nanotubes*, 1st Ed. (World Scientific, Singapore, 1998).

⁶ R. F. Rajter, R. Podgornik, V. A. Parsegian, R. H. French, and W. Y. Ching, *Phys. Rev. B* **76**, 045417 (2007).

⁷ A. Šiber, R. F. Rajter, R. H. French, W. Y. Ching, V. A. Parsegian, and R. Podgornik, *Phys. Rev. B* **80**, 165414 (2009).

⁸ M. S. Dresselhaus, G. Dresselhaus, K. Sugihara, I. A. Spain, H. A. Goldberg, *Graphite Fibers and Filaments* (Springer Series in Materials Science), 1st Ed. (Springer, 1988).

⁹ J.-C. Charlier, X. Gonze, J.-P. Michenaud, *Carbon* **32**, 289 (1994).

¹⁰ J.-C. Charlier, X. Gonze and J.-P. Michenaud, *Europhys. Lett.* **28**, 403 (1994).

¹¹ A. N. Kolmogorov and V. H. Crespi, *Phys. Rev. B* **71**, 235415 (2005); *Phys. Rev. Lett.* **85**, 4727 (2000).

¹² R. H. French, V. A. Parsegian, R. Podgornik et al., *Rev. Mod. Phys.* **82**, 1887 (2010).

¹³ A. Bostwick, T. Ohta, T. Seyller, K. Horn and E. Rotenberg, *Nature Phys.* **3**, 36 (2007); Z. Q. Li, E. A. Henriksen, Z. Jiang, Z. Hao, M. C. Martin, P. Kim, H. L. Stormer and D. N. Basov, *Nature Physics* **4**, 532 (2008).

¹⁴ X. Du, I. Skachko, F. Duerr, A. Luican and E. Y. Andleria, *Nature* **462**, 192 (2009); K. I. Bolotin, F. Ghahari, M. D. Shulman, H. L. Stormer, P. Kim, *Nature* **462**, 196 (2009).

¹⁵ V.W. Brar et al., *Phys. Rev. Lett.* **104**, 036805 (2010); E.A. Henriksen et al., *ibid* **104**, 067404 (2010); A. Luican, G. Li, and E.Y. Andrei, *Phys. Rev. B* **83**, 041405(R) (2011); K.F. Mak, J. Shan, and T.F. Heinz, *Phys. Rev. Lett.* **106**, 046401 (2011); F. Ghahari et al., *ibid* **106**, 046801 (2011).

¹⁶ A. Bostwick, F. Speck, Th. Seyller, K. Horn, M. Polini, R. Asgari, A. H. MacDonald, E. Rotenberg, *Science* **328**, 999 (2010).

¹⁷ V. N. Kotov, B. Uchoa, V. M. Pereira, A. H. Castro Neto, F. Guinea, arXiv:1012.3484.

¹⁸ Y. Barlas, T. Pereg-Barnea, M. Polini, R. Asgari, and A.H. MacDonald, *Phys. Rev. Lett.* **98**, 236601 (2007).

¹⁹ M. Polini, R. Asgari, Y. Barlas, T. Pereg-Barnea, and A. H. MacDonald, *Solid State Commun.* **143**, 58 (2007); M. Polini, R. Asgari, G. Borghi, Y. Barlas, T. Pereg-Barnea,

- and A. H. MacDonald, Phys. Rev. B **77**, 081411(R) (2008); A. Qauimzadeh, R. Asgari, Phys. Rev. B **79**, 075414 (2009); New J. Phys. **11** 095023 (2009); A. Qauimzadeh, N. Arabchi and R. Asgari, Solid State Commun. **147**, 172 (2008).
- ²⁰ E.H. Hwang and S. Das Sarma, Phys. Rev. B **75**, 205418 (2007); S. Das Sarma, E.H. Hwang, and W.-K. Tse, Phys. Rev. B **75**, 121406(R) (2007); E.H. Hwang, B.Y.-K. Hu, and S. Das Sarma, Phys. Rev. B **76**, 115434 (2007) and Phys. Rev. Lett. **99**, 226801 (2007).
- ²¹ M. Polini, A. Tomadin, R. Asgari, and A. H. MacDonald, Phys. Rev. B **78**, 115426 (2008).
- ²² V. A. Parsegian, *Van der Waals Forces* (Cambridge University Press, Cambridge, 2005); M. Bordag, G. L. Klimchitskaya, U. Mohideen, and V. M. Mostepanenko, *Advances in the Casimir Effect* (Oxford University Press, New York, 2009); D. C. Langreth et al., J. Phys.: Condens. Matter **21**, 084203 (2009); T. Emig, Int. J. Mod. Phys. A **25**, 2177 (2010); J. Schwinger, L. L. Deraad, Jr., and K. A. Milton, Ann. Phys. (N.Y.), **115**, 1 (1978).
- ²³ B. E. Sernelius, arXiv:1011.2363v1.
- ²⁴ H. Rydberg et al., Phys. Rev. Lett. **91**, 126402 (2003); J. Rohrer and P. Hyldgaard, arXiv:1010.2925v2.
- ²⁵ G. Veble and R. Podgornik, Phys. Rev. B **75**, 155102 (2007).
- ²⁶ R. Podgornik, P. L. Hansen and V. A. Parsegian, J. Chem. Phys. **119**, 1070 (2003).
- ²⁷ F. Wooten, *Optical Properties of Solids* (Academic Press, New York, 1972).
- ²⁸ B. Wunsch, T. Stauber, F. Sols, and F. Guinea, New J. Phys. **8**, 318 (2006); X.-F. Wang and T. Chakraborty, Phys. Rev. B **75**, 041404 (2007); E.H. Hwang and S. Das Sarma, Phys. Rev. B **75**, 205418 (2007).
- ²⁹ S. Gangadharaiah, A. M. Farid, and E. G. Mishchenko, Phys. Rev. Lett. **100**, 166802 (2008).
- ³⁰ R. Podgornik, R. H. French and V. A. Parsegian, J. Chem. Phys. **124**, 044709 (2006).
- ³¹ B. E. Sernelius and P. Björk, Phys. Rev. B **57**, 6592 (1998).
- ³² J. Mahanty and B. W. Ninham, *Dispersion Forces* (Academic Press, New York, 1976).
- ³³ D. B. Hough and L. R. White, Adv. Colloid Interface Sci. **14**, 3 (1980).